Article

An electrochemical biosensor based on tetrahedral DNA nanostructures and G-quadruplex/hemin conformation for the ultrasensitive detection of microRNA-21 in serum

Jian Lu, Jin Wang, Xialin Hu, Eric Gyimah, Salome Yakubu, Kun Wang, Xiangyang Wu, and Zhen Zhang

Anal. Chem., **Just Accepted Manuscript** • DOI: 10.1021/acs.analchem.9b01133 • Publication Date (Web): 10 May 2019

An Electrochemical Biosensor Based on Tetrahedral DNA Nanostructures and G-quadruplex/hemin Conformation for the Ultrasensitive Detection of MicroRNA-21 in Serum

Jian Lu[1,2], Jin Wang[1,2], Xialin Hu[3], Eric Gyimah[1], Salome Yakubu[1], Kun Wang[4], Xiangyang Wu[1], Zhen Zhang[1]*

[1]School of the Environment and Safety Engineering, Jiangsu University, Zhenjiang 212013, China

[2]Institute of Life Sciences, Jiangsu University, Zhenjiang 212013, China

[3]Key Laboratory of Yangtze River Water Environment, Ministry of Education, College of Environmental Science and Engineering, Tongji University, 1239 Siping Road, Shanghai, 200092, China

[4]The School of Chemistry and Chemical Engineering, Jiangsu University, Zhenjiang 212013, China

E-mail: zhangzhen@ujs.edu.cn (Zhen Zhang).

Fax: +86-511-88790955

ABSTRACT

MicroRNAs (miRNAs) play an important role as significant biomarkers in disease diagnostics. Here, an electrochemical biosensor was developed for the quick, sensitive and specific detection of miRNAs from human serum samples using three-dimensional (3D) DNA tetrahedron-structured probes (TSPs) and duplex-specific nuclease (DSN). The designed TSPs were composed of a recognition sequence that corresponded to a target miRNA and G-quadruplex sequence that was combined with hemin to mimic the biocatalytic functions for H_2O_2 reduction and L-cysteine oxidation. After hybridization with miRNA, the TSPs were immobilized on the Au electrode to shape DNA-RNA double strands, which can be discriminated by DSN for hydrolysing the DNA in the heteroduplexes to generate a significant change in the reduction currents. Under optimal conditions, the biosensor showed a wide linear response ranging from 0.1 fM to 0.1 pM with a low detection limit of 0.04 fM. Meanwhile, the method showed acceptable accuracy and precision for the determination of miRNAs in serum after a series of assessments.

Keywords

MicroRNA detection, duplex-specific nuclease, signal amplification, G-quadruplex/hemin, electrochemical biosensor

MicroRNAs (miRNAs) are a kind of short noncoding RNAs that serve as the critical regulators of gene expression by degrading or blocking mRNAs translation[1-3], and their abnormal expression is closely related to multiple human diseases [4,5], such as cancer[6,7]. Owing to being stale in serum[8,9], miRNAs could be used as promising biomarkers for cancer identification and prognosis. Therefore, it is very important to develop a suitable analytical method to determine miRNAs in the early diagnosis of diseases. However, due to their extremely similar sequences and low expression, establishing a method to identify and quantify miRNAs remains a challenge[10-12].

Some approaches have been reported for miRNA detection, such as the use of microarrays[13], the real-time polymerase chain reaction (RT-PCR)[14,15], Northern blot analysis[16] and in situ hybridization[17], but these methods suffer from some instinctive inefficiencies (e.g., poor sensitivity, complicated operation and high cost)[18] . Thus, a simple, rapid, and sensitive analytical method for miRNA detection is urgently needed.

As well-recognized promising candidates, electrochemical biosensors based on DNA probes are widely used in miRNA detection because of their advantages of high sensitivity, rapid response and simple operation[19-22]. However, a challenge in the design of these biosensors is the control of the density and orientation of the recognition probes, leading to the fact that the binding activity of single strand DNA with the targets is inhibited and the sensitivity and stability of the biosensors might be affected[23-25].

To address this problem, three-dimensional (3D) DNA tetrahedron-structured probes (TSPs) were introduced into the system[15]. As a new type of DNA structure, the TSPs could be attached onto the Au electrode surface as capture probes depending on their

thiolated DNA tetrahedral nanostructures. These probes could provide excellent properties of mechanical rigidity and structural stability[26,27]. In addition, DNAzyme has received great attention as a new type of signal amplification recognition tool. It is a single-stranded nucleotide capable of catalyzing a specific chemical reaction[28]. As a typical DNAzyme, G-quadruplex/hemin formed by interacting hemin into a single-strand guanine-rich nucleic acid sequence, which acts as an horse radish peroxidase (HRP)-mimicking enzyme for electrocatalysis[29,30]. At the same time, the duplex specific nuclease (DSN) can hydrolyze DNA in the DNA-RNA hybrids, while little activity would be against single stranded DNA[31-33], and its property in discriminating perfectly and non-perfectly matched short duplexes contributes to DSN-mediated signal amplification strategy[34,35].

Enlightened by the above literatures, here, a novel electrochemical biosensor was constructed for the quick detection of miRNA based on TSPs and DSN. TSPs were used to control the density and orientation probes at the electrode surface, improving the detection efficiency. Meanwhile, the stable electrochemical signal generated from synergistic effect of G-quadruplex/hemin and L-cysteine and the signal enhancement was achieved by DSN-assisted target recycling. Through a series of assessments, this biosensor successfully carried out target detection in human serum.

EXPERIMENTAL SECTION

Materials and Reagents. All miRNA and DNA sequences were purchased from Sangon Biotechnology Co., Ltd. (Shanghai, China), and the sequences could be seen at Table S1. Hemin was purchased from Macklin Biochemical Co., Ltd. (Shanghai,

China). 6-Mercaptohexanol (MCH) was purchased from Meryer Chemical Technology Co., Ltd. (Shanghai, China). All solutions were prepared with ultrapure water (Milli-Q, 18 MΩ·cm resistivity at 25 °C, Merck Millipore, USA).

Self-Assembly of DNA Tetrahedron-Structured Probes. The TSPs were prepared as reported[15,36,37]: Four strands were dissolved in a Tris-EDTA buffer to get a final concentration of 50 μM. Then, 2 μL of each strand was combined with 37 μL of TM buffer, after which 5 μL of TCEP (30 mM) was added into the solution to prevent the formation of disulfide bonds. The mixture was heated to 95 °C and kept this temperature about 2 min, then incubated at 37 °C for 30 min, and finally cooled to 4 °C and retained over 30 s with BioRad thermal cycler PTC-100 equipment.

Construction of DNA Tetrahedron-Structured Probe-Based Biosensors. Au electrodes with diameters of 2 mm (CH Instruments, Austin, TX, USA) were cleaned following the reported protocol[38,39]. Then, 3 μL of prepared TSPs solution (1 μM) was dropped onto the freshly cleaned surface of the Au electrode and allowed to react overnight at room temperature. 3 μL of MCH (1 mM) was added dropwise onto the Au electrode surface and incubated at 4 °C for 30 min to block the nonspecific binding sites. The obtained electrode was incubated with 3 μL hemin (1 mM) for a definite time at room temperature, and the electrode was labeled as the hemin/ G-quadruplex/ TSPs/ Au electrode.

MiRNA Detection. A total of 2 μL of miRNA-21 with various concentrations and 1 μL DSN were applied to the electrode. After 1 h incubation at 65 ℃, the electrode was rinsed to ensure readiness for the electrochemical measurements.

Electrochemical Measurements. The electrochemical impedance spectroscopy (EIS) measurements were performed using a Model CHI 660E electrochemical workstation (CH Instruments, Inc., Austin, TX). A three-electrode system with an Au working electrode, an Ag/AgCl reference electrode, and a platinum wire counter electrode were used throughout the experiments. The measurement range for cyclic voltammetry (CV) was −0.2 to 0.6 V at a scan rate of 100 mV/s. Differential pulse voltammetry (DPV) experiments were implemented over the range of −0.6 to 0 V in PBS (10 mM, pH 7.0) including L-cysteine with a definite concentration.

RESULTS AND DISCUSSION

Detection Strategy of the Biosensor. As shown in Figure 1, 3D DNA TSPs were decorated on the Au electrode by Au-S bond. At the end of TSPs, the G-quadruplex/hemin was used as a synergistic pseudo-bioenzyme. Under aerobic conditions, H_2O_2 can be generated via the oxidation process of L-cysteine. Then, the G-quadruplex/hemin catalyzed the reduction of H_2O_2 to H_2O, and hemin (Red) was oxidized to hemin (Ox) simultaneously. When incubated with miRNA-21, the TSPs were combined with target miRNA and shaped DNA-RNA double strands, which will be specifically cleaved by DSN. The released miRNA can participate in the next recycle[15,40,41], resulting in a significant current reduction, contributing to obtaining a satisfactory sensitivity of the established biosensor.

Characterization of the Modified Electrode. CV measurements were constructed in 5.0 mM of $[Fe(CN)_6]^{3-/4-}$ to fabricate the electrode surface at each step (displayed by Figure 2A). Curve b indicated that the peak current of the TSPs/Au electrode

declined distinctly in comparision with the bare Au electrode (revealed by curve a). Seen from curve c, while the TSPs/Au electrode was blocked by MCH, the signal was dropped correspondingly. Meanwhile, another decreased peak current was observed (curve d) after incubation with hemin. Through further treatment with miRNA-21 in the presence of DSN, the peak current increases and the peak-to-peak separation declined (curve e).

EIS measurements were also implemented to further provide information about the preparation of the biosensor[42]. Figure 2B indicated that the bare Au electrode displayed an extremely narrow semicircle (curve a). When treated with the TSPs on the Au electrode surface, the Ret of the Au electrode was enhanced, because the path of electron transport was blocked (curve b). Then, the Ret further increased (curve c) by blocking with MCH. After treatment with hemin, a significantly increased Ret was also observed (curve d), indicating the successful formation of the G-quadruplex/hemin. Subsequently, the hemin/G-quadruplex/TSPs/Au electrode was treated with a mixture of miRNA-21 and DSN. As expected, the diameter of the semicircle decreased dramatically (curve e), revealing the implementation of the DSN-assisted target recycling strategy. These results showed that the biosensor has been modified successfully on the basis of Figure 1.

Feasibility of the Established Biosensor. The feasibility of the electrochemical biosensing of miRNA was demonstrated by measuring DPV responses under different conditions (Figure 3). In the absence of L-cysteine or hemin, a negligible response was observed (curve b and curve c). By comparison, in the presence of L-cysteine and hemin,

a significant response appeared (curve a), indicating the formation of G-quadruplex/hemin and the essential part of L-cysteine in this analysis system. Moreover, when the hemin/G-quadruplex/TSPs/Au electrode is incubated with miRNA and DSN, significant changes in the reduction peak will appear (curve d), which was due to the hydrolysis of the DNA-RNA duplex and the recycling of miRNA. All the above results clearly demonstrated that our method might provide a new tool for rapid detection of miRNA.

Optimization of Experimental Conditions. To achieve the best analytical performance, several parameters that could potentially affect the method were systematically investigated (including the concentrations of TSPs, hemin, L-cysteine, and DSN and the incubation time of DSN).

The density of TSPs immobilized on the electrode was studied by controlling the concentration of TSPs that was added on the electrode surface. As shown in Figure 4, different concentrations of TSPs ranging from 0.4 μM to 1.4 μM were assessed to modify the bare Au electrodes. Figure 4A showed that the peak current went up when TSPs increased in this system, but the peak current remained constant until its concentration reached 1.0 μM. Therefore, 1.0 μM TSPs was chosen as the optimal concentration to modify the Au electrode. Meanwhile, since the electrochemical signal was decided by hemin and L-cysteine, it is necessary to evaluate the effects of both factors. As observed in Figure 4B, the maximum DPV values were obtained when the concentration of hemin reached 1.0 mM. Our results also showed that 3.0 mM was the optimized concentration for L-cysteine (Figure 4C).

In addition, the reaction time and concentration of DSN are also important in the analysis system. As shown in Figure 4D, the signal response decreased with increasing reaction time and reached a plateau after incubation for 60 min. Therefore, a reaction time of 60 min was chosen for DSN-assisted target recycling. Furthermore, the concentration of DSN was also optimized to be 0.01 U for achieving high analytical performance of this sensing system (Figure 4E).

Assay Performance. Under optimal conditions, the sensing platform was incubated with different concentrations of miRNA-21 and evaluated by DPV. As displayed in Figure 5A, the peak currents gradually diminished with increased target. The plot of the response versus the logarithm of the miRNA showed good linearity in the range from 0.1 fM to 0.1 pM following the linear regression equation of $\Delta I = 39.65 \log C + 861.5$ ($\Delta I = I_0 - I$, I and I_0 are related to the peak current when the target exists or not) with a correlation coefficient of 0.9983 (Figure 5B). The detection limit was calculated to be 0.04 fM (S/N=3), which is lower than the values in the previous report (Table S2).

Selectivity. To investigate the selectivity of this established sensor, single-base mismatch, three-base mismatch, and noncomplementary sequences were used to replace the targets. Figure 6 revealed the comparison of the DPV responses of the target and mismatched miRNAs. The ΔI of the mismatched sequences is much lower than the target miRNAs. In addition, when miRNA-21 and other miRNAs were mixed in the solution, the DPV response was almost identical to that the miRNA-21 was only present. The results demonstrated that the developed biosensor could be applied to distinguish different miRNA sequences.

Reproducibility and Stability. The reproducibility of the established method has been evaluated. Six modified electrodes were used to detect miRNA-21(1 nM), and the relative standard deviation is 2.0% (Figure 7). Shown that the biosensor had good reproducibility.

The stability of the detection system has also been evaluated. Three modified electrodes were storage at 4 C over 2 weeks before measurement. The results displayed that the modified electrode could retain about 94.2%, implying that the developed electrochemical biosensor had satisfactory stability.

Method Verification and Real Sample Analysis.

In order to verify the accuracy of the approach, a spike-recovery has been implemented using 1% human serum that was diluted by PBS solutions fortified with a variety of miRNAs. Table S3 exhibited that the recoveries of miRNA were in the range of 75.9- 112.2% (RSD, 3.7%- 5.3%), indicating that the accuracy of our method was acceptable.

The proposed biosensor was applied for determine miRNA in human serum that was sampled from 5 newly diagnosed breast cancers. All serum samples were centrifuged from the blood sample at 3000r/ min for 1 minute, together with measurement by a commercial qRT-PCR kit as a reference. As displayed in Table S4, the data from the biosensor agreed well with those measured by qRT-PCR. Accordingly, the proposed electrochemical biosensor can directly measure the concentrations of miRNA-21 in human serum samples and excellent practical utility of this method is demonstrated.

CONCLUSIONS

In summary, a novel electrochemical biosensor was established for sensitive detection of miRNA from human serum. The ultrahigh sensitivity originates from the design of triple signal amplification in the established biosensor, which were based on three-dimensional (3D) DNA tetrahedron-structured probes (TSPs), duplex-specific nuclease (DSN) and G-quadruplex/hemin conformation. Through parameter optimization and evaluation, the proposed biosensor indicated good selectivity, satisfactory sensitivity (LOD, 0.04 fM) and acceptable accuracy. In addition, the expression levels of miRNA-21 in clinical serum samples from cancer patients were evaluated with acceptable results. Therefore, we believe that this work could benefit research on biosensing and clinical assays in terms of its excellent detection performance.

ASSOCIATED CONTENT

Supporting Information

The Supporting Information is available free of charge on the ACS Publications website at DOI: 10.1021/acs.analchem.XXXXXXX

ACKNOWLEDGMENTS

This work was financially supported by the National Natural Science Foundation of China (Grants Nos. 21577051, 21876067, 41601552).

REFERENCES

(1) Fabian, M. R.; Sonenberg, N.; Filipowicz, W. *Annu. Rev. Biochem* **2010**, *79*, 351-379.

(2) Fededa, J. P.; Esk, C.; Mierzwa, B.; Stanyte, R.; Yuan, S.; Zheng, H.; Ebnet, K.; Yan, W.; Knoblich, J. A.; Gerlich, D. W. *The EMBO journal* **2016**, *35*, 2386-2398.

(3) Bo, B.; Zhang, T.; Jiang, Y.; Cui, H.; Miao, P. *Anal. Chem.* **2018**, *90*, 2395-2400.

(4) Hébert, S. S.; De Strooper, B. *Science* **2007**, *317*, 1179.

(5) Huang, J.; Wang, Y.; Guo, Y.; Sun, S. *Hepatology* **2010**, *52*, 60-70.

(6) Pencheva, N.; Tran, H.; Buss, C.; Huh, D.; Drobnjak, M.; Busam, K.; Tavazoie, S. F. *Cell* **2012**, *151*, 1068-1082.

(7) Lu, Z.; Liu, M.; Stribinskis, V.; Klinge, C. M.; Ramos, K. S.; Colburn, N. H.; Li, Y. *Oncogene* **2008**, *27*, 4373.

(8) Grasedieck, S.; Sorrentino, A.; Langer, C.; Buske, C.; Döhner, H.; Mertens, D.; Kuchenbauer, F. *Blood* **2013**, *121*, 4977.

(9) Weber, J. A.; Baxter, D. H.; Zhang, S.; Huang, D. Y.; How Huang, K.; Jen Lee, M.; Galas, D. J.; Wang, K. *Clin. Chem.* **2010**, *56*, 1733.

(10) Wang, M.; Zhou, Y.; Yin, H.; Jiang, W.; Wang, H.; Ai, S. *Biosens. Bioelectron.* **2018**, *107*, 34-39.

(11) Wang, M.; Fu, Z.; Li, B.; Zhou, Y.; Yin, H.; Ai, S. *Anal. Chem.* **2014**, *86*, 5606-5610.

(12) Wang, M.; Yin, H.; Zhou, Y.; Sui, C.; Wang, Y.; Meng, X.; Waterhouse, G. I. N.;

Ai, S. *Biosens. Bioelectron.* **2019**, *128*, 137-143.

(13) Thomson, J. M.; Parker, J.; Perou, C. M.; Hammond, S. M. *Nature methods* **2004**, *1*, 47-53.

(14) Shi, R.; Chiang, V. L. *Biotechniques* **2005**, *39*, 519-525.

(15) Xu, F.; Dong, H.; Cao, Y.; Lu, H.; Meng, X.; Dai, W.; Zhang, X.; Al-Ghanim, K. A.; Mahboob, S. *ACS Appl Mater Interfaces* **2016**, *8*, 33499-33505.

(16) Válóczi, A.; Hornyik, C.; Varga, N.; Burgyán, J.; Kauppinen, S.; Havelda, Z. *Nucleic Acids Res.* **2004**, *32*, e175-e175.

(17) Deo, M.; Yu, J. Y.; Chung, K. H.; Tippens, M.; Turner, D. L. *Dev Dyn* **2006**, *235*, 2538-2548.

(18) Hunt, E. A.; Broyles, D.; Head, T.; Deo, S. K. *Annu Rev Anal Chem* **2015**, *8*, 217-237.

(19) Wang, J.; Lu, J.; Dong, S.; Zhu, N.; Gyimah, E.; Wang, K.; Li, Y.; Zhang, Z. *Biosens. Bioelectron.* **2019**, *130*, 81-87.

(20) Su, S.; Wu, Y.; Zhu, D.; Chao, J.; Liu, X.; Wan, Y.; Su, Y.; Zuo, X.; Fan, C.; Wang, L. *Small* **2016**, *12*, 3794-3801.

(21) Zhang, Z.; Dong, S.; Ge, D.; Zhu, N.; Wang, K.; Zhu, G.; Xu, W.; Xu, H. *Biosens. Bioelectron.* **2018**, *105*, 77-80.

(22) Liang, Y.-R.; Zhang, Z.-M.; Liu, Z.-J.; Wang, K.; Wu, X.-Y.; Zeng, K.; Meng, H.; Zhang, Z. *Biosens. Bioelectron.* **2017**, *91*, 199-202.

(23) Irving, D.; Gong, P.; Levicky, R. *J Phys Chem B* **2010**, *114*, 7631-7640.

(24) Chen, X.; Zhou, G.; Song, P.; Wang, J.; Gao, J.; Lu, J.; Fan, C.; Zuo, X. *Anal.*

Chem. **2014**, *86*, 7337-7342.

(25) Peng, G.; Li, X.; Cui, F.; Qiu, Q.; Chen, X.; Huang, H. *ACS Appl Mater Interfaces* **2018**, *10*, 17551-17559.

(26) Lu, H.-J.; Pan, J.-B.; Wang, Y.-Z.; Ji, S.-Y.; Zhao, W.; Luo, X.-L.; Xu, J.-J.; Chen, H.-Y. *Anal. Chem.* **2018**, *90*, 10434-10441.

(27) Xie, N.; Huang, J.; Yang, X.; He, X.; Liu, J.; Huang, J.; Fang, H.; Wang, K. *Anal. Chem.* **2017**, *89*, 12115-12122.

(28) Huang, J.-Y.; Zhao, L.; Lei, W.; Wen, W.; Wang, Y.-J.; Bao, T.; Xiong, H.-Y.; Zhang, X.-H.; Wang, S.-F. *Biosens. Bioelectron.* **2018**, *99*, 28-33.

(29) Zhou, Y.-C.; Ran, X.-X.; Chen, A.-Y.; Chai, Y.-Q.; Yuan, R.; Zhuo, Y. *Anal. Chem.* **2018**, *90*, 9109-9116.

(30) Li, H.; Chang, J.; Gai, P.; Li, F. *ACS Appl Mater Interfaces* **2018**, *10*, 4561-4568.

(31) Zhang, K.; Wang, K.; Zhu, X.; Xu, F.; Xie, M. *Biosens. Bioelectron.* **2017**, *87*, 358-364.

(32) Ren, Y.; Deng, H.; Shen, W.; Gao, Z. *Anal. Chem.* **2013**, *85*, 4784-4789.

(33) Huo, X.-L.; Zhang, N.; Yang, H.; Xu, J.-J.; Chen, H.-Y. *Anal. Chem.* **2018**, *90*, 13723-13728.

(34) Lee, J. H.; Kim, J. A.; Jeong, S.; Rhee, W. J. *Biosens. Bioelectron.* **2016**, *86*, 202-210.

(35) Qiu, X.; Zhang, H.; Yu, H.; Jiang, T.; Luo, Y. *Trends Biotechnol* **2015**, *33*, 180-188.

(36) Wen, Y.; Pei, H.; Wan, Y.; Su, Y.; Huang, Q.; Song, S.; Fan, C. *Anal. Chem.* **2011**,

83, 7418-7423.

(37) Weber, J. A.; Baxter, D. H.; Zhang, S.; Huang, D. Y.; Huang, K. H.; Lee, M. J.; Galas, D. J.; Wang, K. *Clin. Chem.* **2010**, *56*, 1733-1741.

(38) Zhang, J.; Song, S.; Wang, L.; Pan, D.; Fan, C. *Nat Protoc* **2007**, *2*, 2888-2895.

(39) Lao, R.; Song, S.; Wu, H.; Wang, L.; Zhang, Z.; He, L.; Fan, C. *Anal. Chem.* **2005**, *77*, 6475-6480.

(40) Huo, X. L.; Yang, H.; Zhao, W.; Xu, J. J.; Chen, H. Y. *ACS Appl Mater Interfaces* **2017**, *9*, 33360-33367.

(41) Xia, N.; Liu, K.; Zhou, Y.; Li, Y.; Yi, X. *Int J Nanomedicine* **2017**, *12*, 5013-5022.

(42) Xiong, E.; Zhang, X.; Liu, Y.; Zhou, J.; Yu, P.; Li, X.; Chen, J. *Anal. Chem.* **2015**, *87*, 7291-7296.

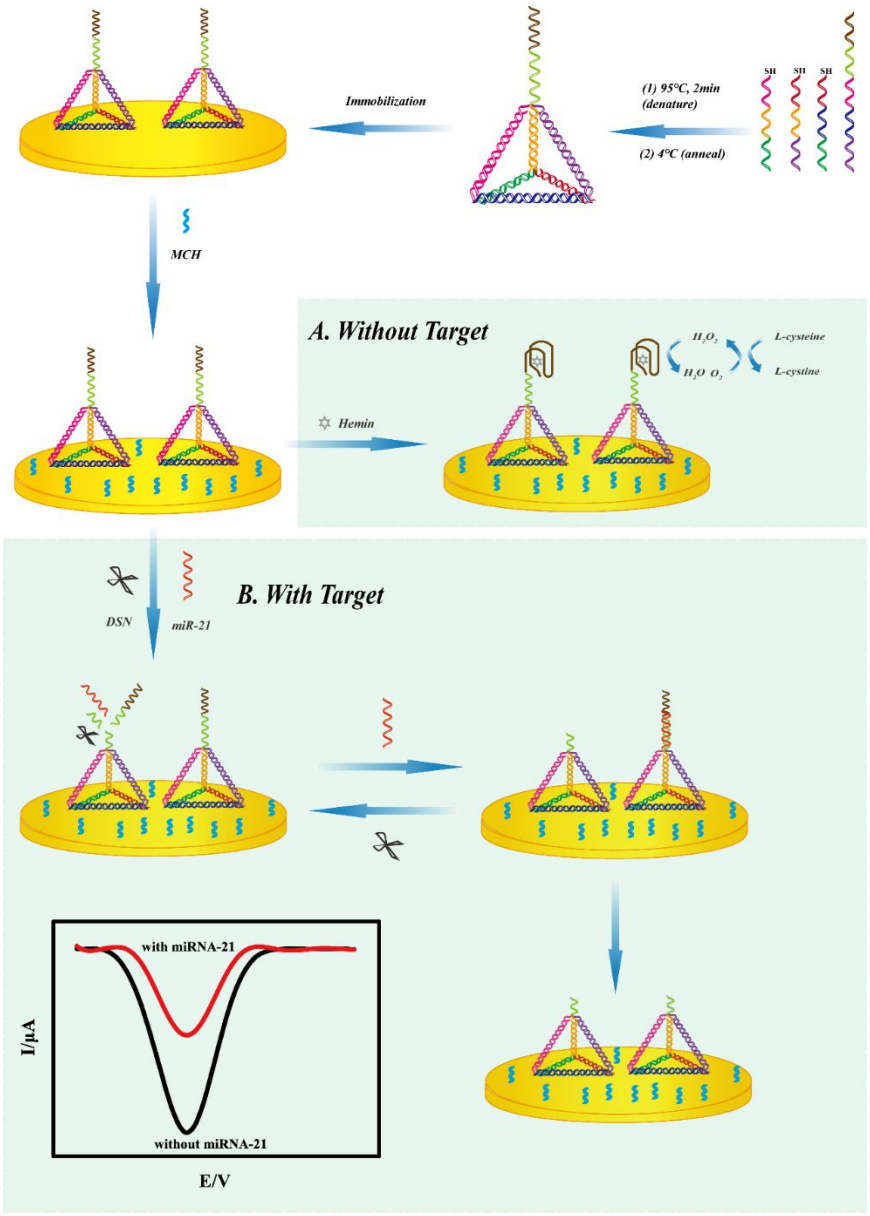

Figure 1. Schematic illustration of the electrochemical biosensor for the detection of miRNA-21.

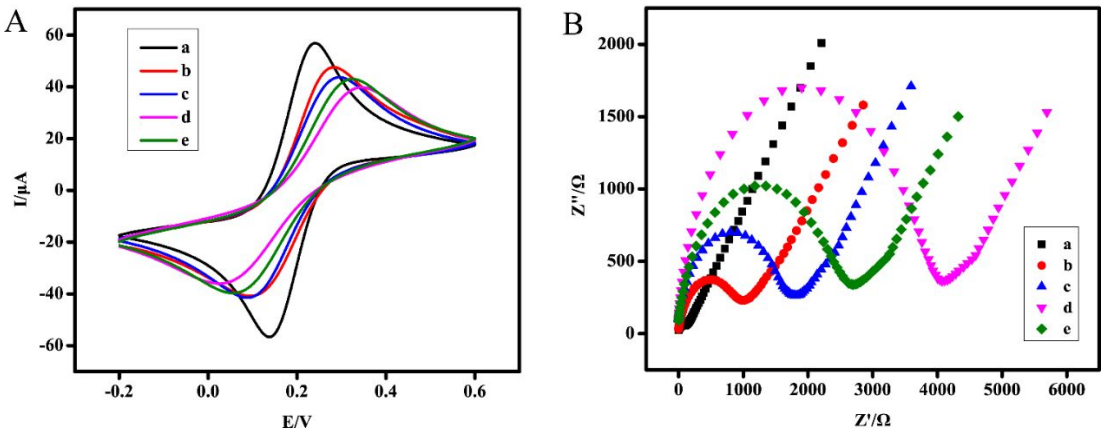

Figure 2. Cyclic voltammograms (A) and Nyquist plots (B) of the developed biosensor. (**a**) Bare Au electrode, (**b**) TSPs/Au electrode, (**c**) MCH/TSPs/Au electrode, (**d**) hemin/MCH/TSPs/Au electrode, (**e**) hemin/MCH/TSPs/Au electrode after reacted with miRNA/DSN.

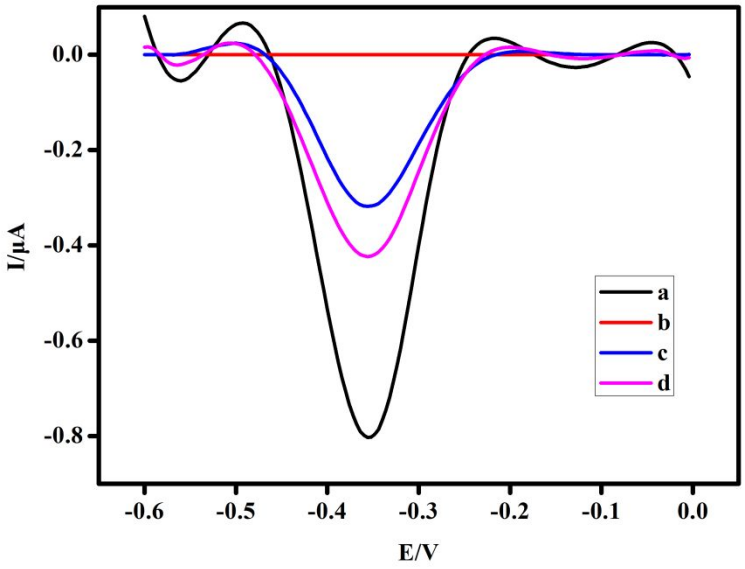

Figure 3. DPV results of (a) L-cysteine/hemin/MCH/TSPs/Au electrode, (b) L-cysteine/MCH/TSPs/Au electrode, (c) hemin/MCH/TSPs/Au electrode, and (d) L-cysteine/hemin/MCH/TSPs/Au electrode after reacted with miRNA/DSN.

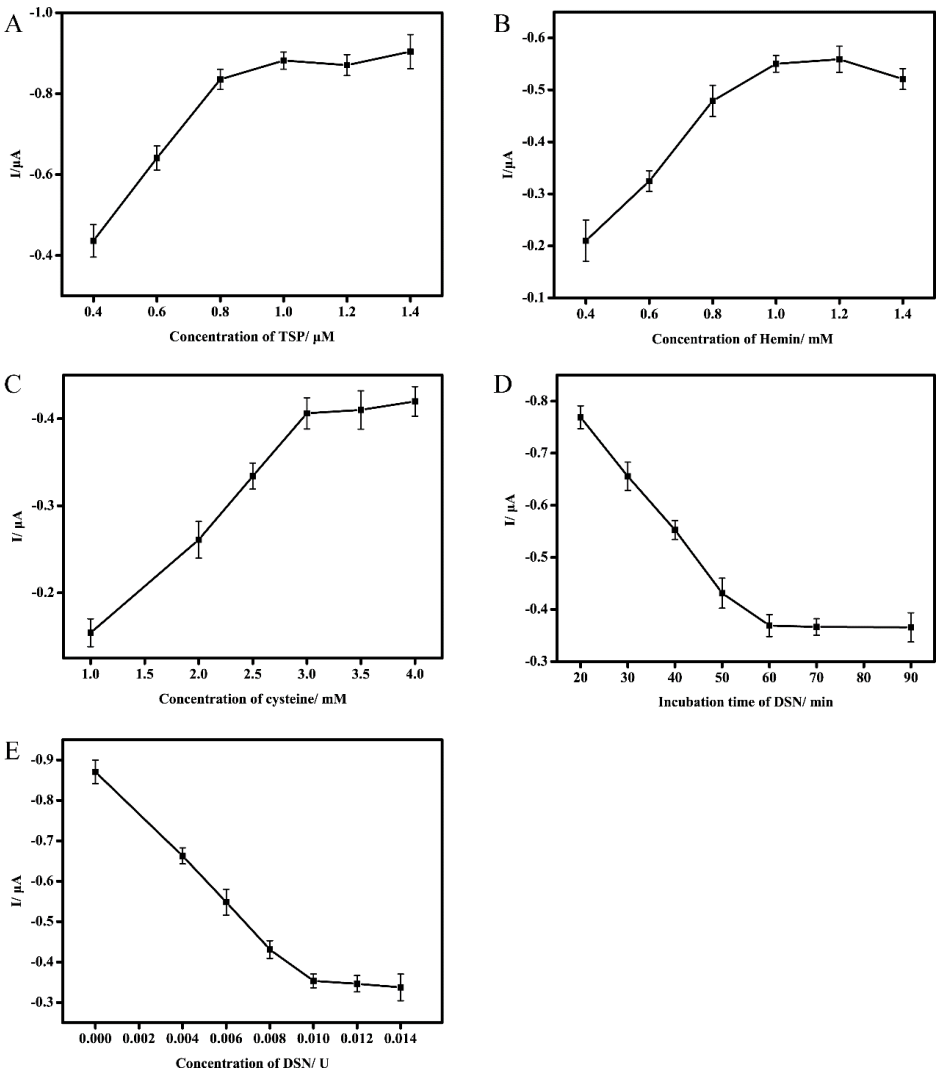

Figure 4. Effects of TSPs concentration on DPV response (A); Effects of concentration of Hemin on DPV response (B); Effects of cysteine concentration on DPV response (C); Effects of incubation time of DSN on DPV response (D); Effects of DSN concentration on DPV response (E).

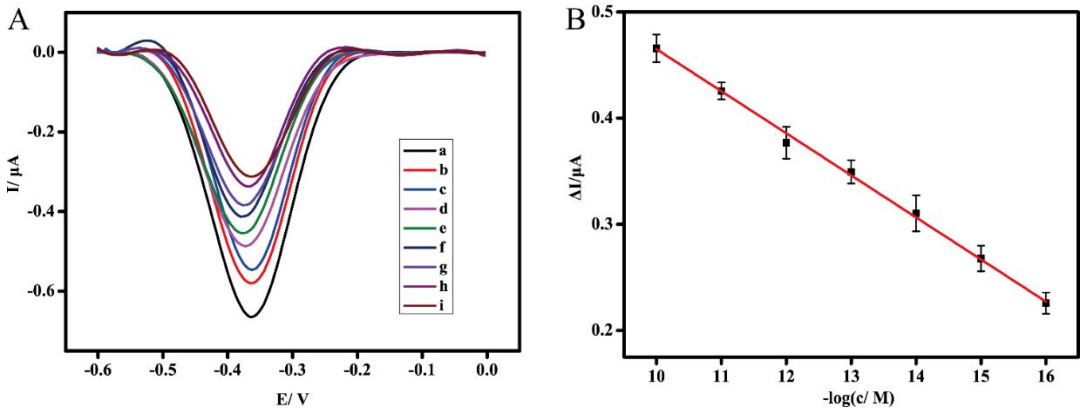

Figure 5. DPV curves responding to different miRNA concentrations (from a to i): 0, 1.0×10^{-16}, 1.0×10^{-15}, 1.0×10^{-14}, 1.0×10^{-13}, 1.0×10^{-12}, 1.0×10^{-11}, 1.0×10^{-10} M, 1.0×10^{-9} M, respectively (A); The linear relationship between the current variation ΔI and the negatively logarithm of the miRNA concentration (B).

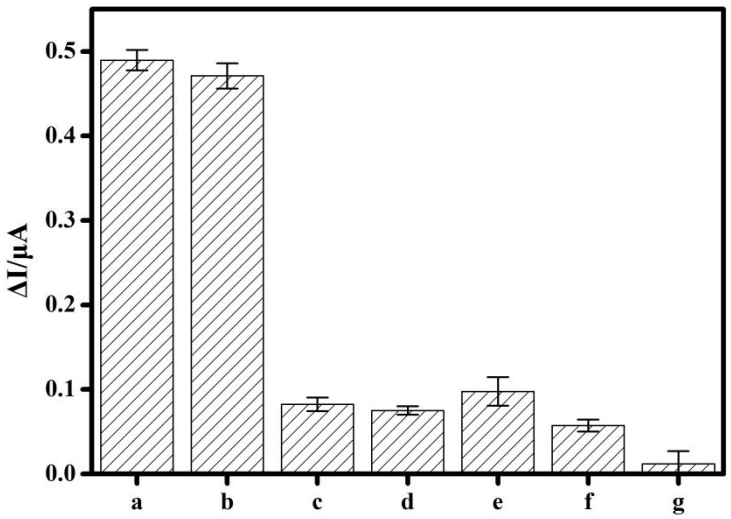

Figure 6. The selectivity of the sensor hybridized to different miRNA sequences: (a) miRNA-21; (b) mixture of miRNA-21, miRNA-21a, miRNA-21b, miRNA-21c, three-base mismatched miRNA-21 and noncomplementary miRNA-21; (c) single-base mismatched miRNA-21a; (d) single-base mismatched miRNA-21b; (e) single-base

mismatched miRNA-21c; (f) three-base mismatched miRNA-21; (g) noncomplementary miRNA-21.

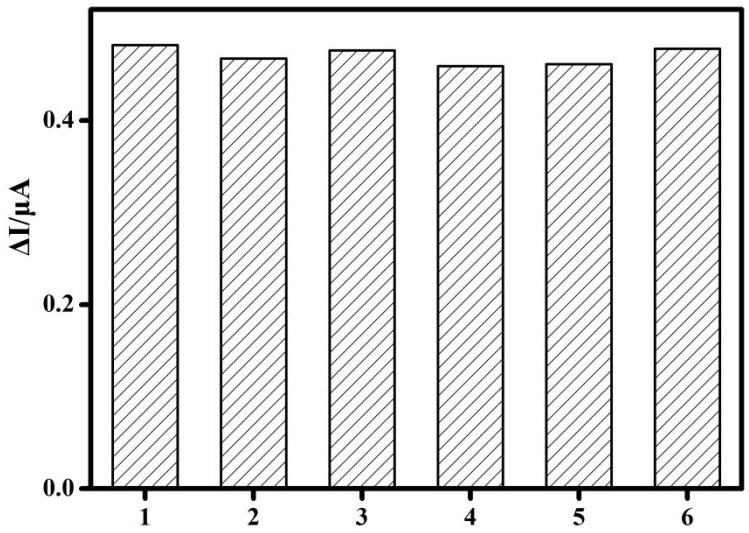

Figure 7. The reproducibility of the established biosensor.

Graphical Abstract